Ecotoxicology and Environmental Safety 323 (2026) 120751

Contents lists available at ScienceDirect

Ecotoxicology and Environmental Safety

journal homepage: www.elsevier.com/locate/ecoenv

Chronic paternal Wi-Fi RF-EMR exposure impairs placental efficiency and fetal growth: Association with sex-dependent histone modification patterns in mice

Jun Wang [1], Lingxia Gao [1], Ni Jin [1], Song Yan, Hui Lei, Ying Ju, Shuqiang Chen [*], Xiaohong Wang [*]

Department of Obstetrics and Gynecology, Tangdu Hospital, Fourth Military Medical University, Xi'an, China

ARTICLE INFO

Keywords:
Wi-Fi
RF-EMR
Sperm quality
Placental efficiency
Histone modification
Sexdependent

ABSTRACT

The widespread use of Wi-Fi-derived radiofrequency electromagnetic radiation (RF-EMR) has raised concerns regarding male reproductive health; however, whether paternal exposure exerts transgenerational effects on offspring development remains unclear. This study investigated the effects of chronic paternal 2.4 GHz Wi-Fi RF-EMR exposure (whole-body SAR 0.125–0.5 W/kg, 4 h/day, 6 days/week for 20 weeks) on sperm quality in F0 male mice and placental development in F1 offspring, with a focus on epigenetic regulation. Paternal RF-EMR exposure significantly reduced sperm concentration and increased the sperm abnormality rate in F0 males. F1 offspring exhibited reduced fetal weight and placental efficiency, with more pronounced impairments in male offspring. Mechanistically, paternal exposure reduced the proportion of placental labyrinth layer and down-regulated multiple nutrient transporters in a male-biased manner. Epigenetic analysis revealed sex-dependent histone modifications in placentas following paternal RF-EMR exposure: male placentas exhibited increased H3K9me2/3, H3K27me3, H3K27ac, and H3K4me2, whereas female placentas exhibited decreased H3K4me2. ChIP-qPCR targeting transporter promoters revealed sex-specific enrichment of repressive histone marks in placentas from exposed fathers. In male placentas, H3K27me3 was increased at the *Atp1a1* and *Slc22a3* promoters, and H3K9me3 was increased at the *Atp1a1* and *Slc2a1* promoters. In female placentas, H3K27me3 at the *Slc3a2* promoter was significantly decreased. Collectively, chronic paternal Wi-Fi RF-EMR exposure impairs fetal growth and placental efficiency, with male offspring being more susceptible, and is associated with disrupted placental structure, impaired nutrient transport, and sex-dependent histone modifications in the offspring placenta. These findings underscore the importance of considering paternal RF-EMR exposure in reproductive risk assessment.

1. Introduction

Wi-Fi has become an indispensable technology in modern society, with widespread use in both daily life and professional settings. However, the continuous emission of radiofrequency electromagnetic radiation (RF-EMR) from Wi-Fi devices has raised widespread concerns regarding its potential environmental and health effects (Pall, 2018). Unlike mobile phones, which primarily cause localized exposure, Wi-Fi routers typically result in whole-body RF-EMR exposure (Jaffar et al., 2019). Mounting epidemiological and experimental evidence indicates that chronic exposure to Wi-Fi-derived RF-EMR is associated with multiple adverse effects, including cognitive dysfunction, metabolic disorders, and reproductive impairment (Pall, 2018; Sage and Burgio, 2018). Notably, the World Health Organization (WHO) commissioned 12 systematic reviews and meta-analyses to evaluate the health effects of RF-EMR. Most of these reviews were limited by significant methodological shortcomings, including the omission of eligible studies, heterogeneity among primary studies, and inappropriate subgroup analyses, thereby limiting their ability to reliably confirm the safety of wireless communication devices (Melnick et al., 2025). Among these assessments, the review of animal carcinogenicity provided high-certainty evidence for heart schwannomas and moderate-certainty

* Correspondence to: No.1, Xinsi Road, Baqiao District, Xi'an, Shaanxi Province 710000, China.
E-mail addresses: chenshuqiang2012@163.com (S. Chen), wangxh919@fmmu.edu.cn (X. Wang).
[1] These authors contributed equally to this work and share first authorship.

https://doi.org/10.1016/j.ecoenv.2026.120751
Received 15 April 2026; Received in revised form 8 July 2026; Accepted 31 August 2026
Available online 3 September 2026
0147-6513/© 2026 The Author(s). Published by Elsevier Inc. This is an open access article under the CC BY license (http://creativecommons.org/licenses/by/4.0/).

evidence for gliomas, whereas reviews focusing on male fertility and pregnancy outcomes consistently demonstrated dose-dependent adverse reproductive effects (Melnick et al., 2025). Collectively, these findings highlight the need to optimize exposure guidelines and mitigate the reproductive health risks associated with RF-EMR (Melnick et al., 2025).

The male reproductive system is particularly sensitive to RF-EMR exposure, with testicular tissue exhibiting vulnerability comparable to that of neural and dermal tissues (Vijay et al., 2025). Clinical studies have consistently linked Wi-Fi exposure to impaired sperm quality, characterized by reduced progressive motility and increased DNA fragmentation in human spermatozoa (Avendano et al., 2012; Ding et al., 2018; Bektas and Dasdag, 2025). Animal studies have further demonstrated that RF-EMR disrupts the hypothalamic-pituitary-gonadal axis, leading to decreased serum levels of follicle-stimulating hormone and testosterone in rodents (Maluin et al., 2024; Khoshbakht et al., 2021). Histological analyses in mice have shown that RF-EMR exposure reduces seminiferous tubule diameter, epithelial thickness, tubule density, and the number of Sertoli cells (Cakmak et al., 2026). Consequently, exposed males exhibit severe spermatogenic abnormalities, including increased morphological abnormalities and reduced sperm concentration, motility, and viability (Vijay et al., 2025; Maluin et al., 2024; Khoshbakht et al., 2021; Dasdag et al., 2015a).

Beyond direct tissue toxicity, RF-EMR may disrupt cellular functions through epigenetic mechanisms (Abtin et al., 2024; Giorgi and Del Re, 2021; Cantu et al., 2023). Epigenetic modifications—including DNA methylation, histone post-translational modifications, and non-coding RNA expression—mediate environmentally induced phenotypic changes without altering the underlying DNA sequence (Skvortsova et al., 2018). Such epigenetic reprogramming is highly dynamic during germ cell development (Skvortsova et al., 2018; Xavier et al., 2019). Environmental stressors are known to disrupt epigenetic programming in sperm, with adverse consequences for both male fertility and offspring health (Kitamura et al., 2015; Ashapkin et al., 2023; Zhang et al., 2025; Hong et al., 2024). However, whether RF-EMR directly affects sperm epigenetics remains unclear. Current evidence indicates that RF-EMR can alter epigenetic modifications in somatic cells. For example, it alters ERα gene methylation in male Sprague-Dawley rat tissues (Mokarram et al., 2017). It also induces global DNA methylation changes in human keratinocytes (Cantu et al., 2023). In addition, long-term RF-EMR exposure reduces miR-106b-5p and miR-107 levels in the brains of adult male rats (Dasdag et al., 2015b, 2015c), and decreases H3K9me3 levels in the heads of adult Drosophila (Cappucci et al., 2022). Although these observations do not constitute direct evidence in germ cells, they raise the possibility that RF-EMR may similarly alter the epigenetic landscape of sperm, given the shared sensitivity of reproductive and somatic tissues to RF-EMR (Vijay et al., 2025). Collectively, these findings suggest that RF-EMR-induced epigenetic alterations may be transmitted across generations through the paternal germline, warranting further investigation.

Epidemiological studies have also linked paternal RF-EMR exposure to adverse developmental outcomes in offspring. For example, higher paternal exposure to high-frequency antennas is linearly associated with a reduced male-to-female birth ratio (Baste et al., 2008). Additional evidence links paternal RF-EMR exposure to an increased risk of neuroblastoma, preterm birth, preeclampsia, and certain congenital anomalies (De Roos et al., 2001; Mjoen et al., 2006; Blaasaas et al., 2002; Baste et al., 2012). We previously showed that 10-week paternal RF-EMR exposure predisposes male offspring to impaired glucose metabolism in a mouse model (Yan et al., 2022). However, whether chronic paternal Wi-Fi exposure influences intrauterine development through sperm-mediated epigenetic mechanisms remains to be determined.

To date, existing studies have primarily focused on RF-EMR-induced sperm damage, leaving a critical gap in understanding whether chronic paternal Wi-Fi exposure exerts intergenerational effects on placental and fetal development. In particular, no studies have systematically examined whether such paternal exposure leads to sex-specific placental abnormalities or differential susceptibility between male and female offspring. To address this gap, the present study established a 20-week mouse model of chronic paternal exposure to 2.4 GHz Wi-Fi RF-EMR. Our findings demonstrate for the first time that chronic paternal Wi-Fi exposure impairs fetal and placental development in F1 offspring in a sex-specific manner, with male offspring exhibiting more pronounced abnormalities than females, indicating a previously unrecognized male-biased susceptibility in mice.

2. Materials and methods

2.1. Experimental animals

Six-week-old ICR mice were purchased from Beijing Huafukang Laboratory Animal Center (Beijing, China). All animal experiments were approved by the Ethics Committee of Animal and Medicine of Tangdu Hospital, Fourth Military Medical University (Approval No.: SYXK2019–001). Upon arrival, mice were acclimatized for one week under standard laboratory conditions (temperature: 21–23°C, humidity: 50–60%, 12 h light/dark cycle, ventilation frequency: 10–15 times/h) prior to the experiment. Mice had free access to standard mouse chow and sterile tap water throughout both the acclimatization and experimental periods.

2.2. Construction of the Wi-Fi-associated RF-EMR platform

A continuous wave (CW) signal generator (China Electronics Technology Instruments Co., Ltd., China), an amplifier (output power = 8.4 W; SWSPA-C200S/C-2, Chengdu SWIEE Power Electronics Technology Co., Ltd, China), and a horn antenna (gain: 8.94 dB, CW; LB-1080, A-INFO, China) were used to establish the Wi-Fi RF-EMR exposure system. The electromagnetic radiation frequency was set at 2.4 GHz, and mice were allowed free movement within their cages during exposure. The whole-body specific absorption rate (SAR) was measured using a SAR meter (Narda SRM-3006, Narda-Storp, Germany) and calculated based on a prolate spheroidal model of a medium-sized mouse (Yan et al., 2022), yielding a whole-body SAR range of 0.125–0.5 W/kg across different positions within the exposure chamber. The uniformity of the electromagnetic field within the exposure chamber was verified to ensure consistent exposure across all cages.

2.3. Experimental Animal Grouping and Treatment

Male mice were individually housed under the standard conditions described above. The mice were randomly assigned to two groups (n = 20 per group): the radiation exposure group (RE, Wi-Fi-derived RF-EMR) and the sham exposure group (SE). A total of 40 mice were included in this study. Mice in the RE group received daily RF-EMR exposure (4 h/day, 9:00–13:00, with a 15-min break after 2 h of exposure to minimize stress) for 6 consecutive days, followed by 1 day of rest, for a total of 20 weeks. Mice in the SE group were housed in the same exposure chamber with inactive equipment (no RF-EMR emission) to control for non-thermal effects associated with the devices, under otherwise identical conditions as the RE group.

After 20 weeks of exposure, RE and SE male mice were mated with unexposed female ICR mice at a ratio of 1:1. Vaginal plugs were checked daily at 08:00, and the day on which a vaginal plug was detected was designated as 0.5 days post-coitum (dpc). F1 offspring and their placentas were collected at 18.5 dpc for subsequent analyses.

2.4. Hemocytometer-based measurement of sperm concentration in mice

Multiple small incisions were made in the isolated cauda epididymides, which were then immersed in 100 μL of prewarmed HTF medium. The tissues were incubated at 37°C for 10 min to allow passive

swim-out of spermatozoa. The crude sperm suspension was diluted 1:100 with HTF medium. To immobilize motile sperm for accurate counting, the diluted suspension was fixed with 0.4% glutaraldehyde. A coverslip was first placed on the hemocytometer, and 10 μL of the fixed sperm suspension was loaded into the counting chamber through the V-shaped groove to avoid air bubbles. Excess liquid overflowing from the chamber edges was gently removed with filter paper (Sakhaee et al., 2016). The loaded hemocytometer was placed horizontally for 5 min to allow complete sedimentation of the sperm cells. Sperm were counted under a 40 × objective lens (total magnification, ×400) across five diagonal large squares of the counting grid. Only morphologically intact sperm with complete heads and flagella were counted.

Sperm concentration ($\times 10^6$/mL) = (Total sperm count in 5 squares / 5) $\times 2 \times 10^4 \times$ Dilution factor.

Ten mice were included in each group (biological replicates, n = 10 per group). Each diluted sperm sample was loaded and counted three independent times as technical replicates to minimize counting error (Sakhaee et al., 2016).

2.5. Diff-quik staining for morphological analysis of mouse spermatozoa

Briefly, 10 μL of diluted sperm suspension was applied to a pre-cleaned, degreased glass slide, and a thin monolayer smear was prepared by gently dragging the edge of a second glass slide across the sample at a consistent angle to avoid mechanical damage to the sperm flagella. The smear was completely air-dried at room temperature and then fixed by immersion in 95% methanol for 2 min. After fixation, excess methanol was allowed to drain vertically onto filter paper. The slides were sequentially stained by immersion in Diff-Quik Solution 1 (eosinophilic dye) for 20–30 s, followed by Diff-Quik Solution 2 (basophilic dye) for 10–15 s. After each staining step, the slides were held vertically at a 90° angle against absorbent paper to remove excess staining solution before proceeding to the next reagent. Excess dye was gently removed by dipping the slides 5–10 times in distilled water without prolonged soaking to prevent over-decolorization. The slides were completely air-dried under ambient conditions before microscopic examination. Sperm morphology was examined under a 100 × oil immersion objective lens (total magnification, ×1000). For each sample, 100 consecutive spermatozoa were evaluated from at least five randomly selected microscopic fields using a systematic raster-scanning pattern to minimize subjective counting bias. Morphological defects of the sperm head, neck/midpiece, and flagellum were recorded separately.

Under Diff-Quik staining, the acrosomal region of the sperm head appears light blue, the post-acrosomal region appears dark blue, the midpiece appears red, and the tail appears blue or light red. Sperm morphological abnormalities were classified into five categories based on the location of the defect (Ali et al., 2018): (1) immature spermatozoa (presence of cytoplasmic droplets); (2) head abnormalities (double-headed, round-headed, or headless sperm); (3) neck abnormalities (bent or folded necks); (4) tail abnormalities (folded, curled, or short tails); and (5) compound abnormalities (multiple defects in the same spermatozoon). The total malformation rate was calculated as follows: (Number of abnormal sperm / Total sperm counted) × 100%, and the proportion of each abnormality category was also determined.

2.6. Placental Efficiency and Placenta Dissection

The presence of a vaginal plug was used to confirm copulation, and E0.5 was defined as the midpoint of the dark cycle on the day of plug detection. Fetuses and placentas were collected at E18.5. Pregnant mice were euthanized by CO_2 inhalation followed by cervical dislocation. After dissection, placental and fetal wet weights were recorded. Placental efficiency was calculated for each fetus-placenta pair as the ratio of fetal weight to placental weight (fetal weight/placental weight) (Fowden et al., 2009; Hayward et al., 2016), and the litter mean was used for statistical analysis. Each placenta was processed immediately: some were fixed overnight in 4% paraformaldehyde/PBS for histological analyses, whereas the remaining samples were snap-frozen in liquid nitrogen for subsequent mRNA and DNA analyses. For histological and molecular analyses (PAS, IHC, RT-qPCR, Western blot, and ChIP-qPCR), 2–3 placentas were randomly selected from each dam, and at least six placentas from three independent dams per group were included.

2.7. Periodic acid-schiff and immunohistochemical staining for mouse placental tissue analysis

Placental tissues were fixed in 4% paraformaldehyde at 4°C for 24 h, dehydrated through a graded ethanol series (70%, 80%, 90%, 95%, and 100%), and embedded in paraffin. Paraffin Section (5 μm thick) were prepared and stained with Periodic Acid-Schiff (PAS) reagent (AB-PAS, EK, China). Placental morphology was examined, and images were acquired using a digital slide scanner (KF-PRO-005-EX, KFBIO, China).

For immunohistochemical staining, paraffin sections were deparaffinized, rehydrated, and subjected to antigen retrieval (citrate buffer, pH 6.0, 95°C for 20 min). The sections were blocked with 5% bovine serum albumin (BSA) for 30 min at room temperature and then incubated overnight at 4°C with rabbit anti-CD31 antibody (Ab182981, Abcam, UK; 1:200 dilution). After washing with PBS, the sections were incubated with an HRP-conjugated goat anti-rabbit IgG secondary antibody (1:500 dilution) for 1 h at room temperature, followed by DAB chromogenic staining and hematoxylin counterstaining. Images were scanned and collected, and ImageJ software (NIH, USA) was used to quantify the cross-sectional areas of the spongiotrophoblast and labyrinth layers, as well as placental microvascular density (5 random fields per section, 3 sections per placenta).

2.8. Reverse Transcription Quantitative PCR

Placental tissues stored at −80°C were homogenized in Trizol reagent (15596018, Thermo, USA) using an electric tissue grinder (SpeedMill plus, Jena, Germany). Total RNA was extracted by chloroform-isopropanol precipitation (Pharmaceutical Reagent, China), and RNA purity and concentration were determined using a NanoDrop spectrophotometer (Thermo, USA). RNA was reverse-transcribed into cDNA using a reverse transcription kit (RR036A, Takara, China) according to the manufacturer's instructions. Primers for key placental development-related genes and nutrient transporter genes were designed based on the reference sequences of the mouse mm10 genome (sequences listed in Appendix Table 1 and 2) and were commercially synthesized. RT-qPCR was performed using a StepOnePlus real-time quantitative PCR system (ABI, USA) with SYBR Green Master Mix (A6001, Promega, USA). Gapdh was used as the internal reference gene, and relative gene expression levels were calculated using the $2^{-\Delta\Delta CT}$ method. Each sample was analyzed in three technical replicates, and at least three biological replicates per group were included (n ≥ 3).

2.9. Western blot

Histones were extracted from placental tissues stored at −80°C using a histone extraction kit (OP-0006, Epigen Tek, USA) according to the manufacturer's instructions. Protein concentrations were determined using a BCA protein assay kit (P0010, Beyotime, China). Equal amounts of protein (30 μg per lane) were separated by 12% SDS-PAGE and transferred onto PVDF membranes. The membranes were blocked with 5% non-fat milk for 1 h at room temperature and then incubated overnight at 4°C with primary antibodies against H3K4me2, H3K4me3, H3K9me2, H3K9me3, H3K27me3, H3K27ac, and H3 (internal reference). After washing with TBST, the membranes were incubated with HRP-conjugated secondary antibodies for 1 h at room temperature.

Protein bands were visualized using ECL chemiluminescence reagent (Thermo, USA), and band intensities were quantified using ImageJ software. At least three biological replicates per group were included ($n \geq 3$).

2.10. ChIP-qPCR

Mouse E18.5 placental tissues (25 mg) were minced, crosslinked with 1% formaldehyde in PBS for 10 min at room temperature (RT), and quenched with 125 mM glycine on ice for 5 min. After washing, the tissues were homogenized in lysis buffer (SimpleChIP® Plus Sonication Chromatin IP Kit, Cat# 56383, CST) and centrifuged at 12,000 × g for 5 min at 4°C to collect nuclei. The nuclei were lysed, and chromatin was sonicated into fragments of 200–500 bp (50 W, 2 s on/off, 2 min). After centrifugation, the supernatants were incubated overnight at 4°C with anti-H3K27me3 (1:50, #9733S), anti-H3K9me3 (1:50, #13969S), anti-Histone H3 (#4620), or rabbit IgG (#2729). Protein G magnetic beads were then added and incubated for 2 h. The beads were washed with low-salt (3 ×) and high-salt (1 ×) wash buffers. Immunocomplexes were eluted at 65°C for 30 min, reverse-crosslinked in the presence of Proteinase K (0.5 mg/mL) and RNase A (0.2 mg/mL) at 65°C for 2 h, and purified using the kit columns.

qPCR was performed using SYBR Green Master Mix (Cat# CM0139, AG) with promoter-specific primers (see Appendix Table 3). Enrichment was calculated as follows: % Input = 2% × 2^ [(Ct_2% Input - Ct_IP)], where Ct_2% Input represents the Ct value of the 2% input sample.

2.11. Statistical Analysis

All experimental data are presented as the mean ± standard deviation (SD). Statistical analyses and graph generation were performed using GraphPad Prism 8.0.0 (GraphPad Software, Inc., USA). Data normality was assessed using the Shapiro-Wilk test, and homogeneity of variance was evaluated using Levene's test. For all comparisons between the RE and SE groups within the same sex, two-sided independent-samples *t*-tests were performed. Pearson correlation analysis was used to evaluate linear correlations between variables, where applicable. A P value < 0.05 was considered statistically significant. The specific sample sizes (n) for each assay are provided in the corresponding Methods sections and figure legends.

3. Results

3.1. Paternal Wi-Fi RF-EMR impairs sperm quality in F0 male mice

After 20 weeks of exposure to Wi-Fi-derived RF-EMR, male mice in the exposure group exhibited a marked reduction in cauda epididymal sperm concentration, decreasing to $(3.91 \pm 1.59) \times 10^6$/mL compared with $(30.73 \pm 4.32) \times 10^6$/mL in the sham-exposed group ($p < 0.001$) (Fig. 1A).

The total sperm abnormality rate in the RF-EMR exposure (RE) group increased markedly to 89.51%, which was significantly higher than the 29.33% observed in the sham-exposed (SE) group ($p < 0.001$) (Fig. 1B). Notably, the frequencies of head abnormalities (43.36% vs. 4.11%, $p < 0.001$) and compound abnormalities (12.59% vs. 3.07%, $p < 0.001$) were significantly higher in the RE group (Fig. 1C). In contrast, no significant differences were observed between the two groups in the frequencies of immature spermatozoa (2.80% vs. 3.64%, $p = 0.533$) or neck abnormalities (16.08% vs. 15.48%, $p = 0.724$) (Fig. 1C).

3.2. Paternal RF-EMR Reduces Fetal Weight and Placental Efficiency in Offspring

At 18.5 days post-coitum (dpc), litter size, fetal and placental weights (stratified by sex), and placental efficiency (fetal-to-placental weight ratio) were compared between the RE and SE groups. As shown in

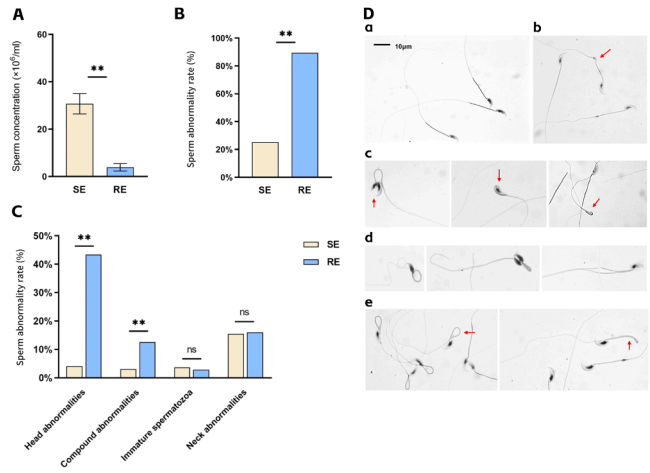

Fig. 1. Effects of Wi-Fi-derived RF-EMR exposure on sperm parameters in F0 male mice. (A) Sperm concentration in the cauda epididymis of sham-exposed (SE) and RF-EMR-exposed (RE) male mice. (B) Total sperm abnormality rate in SE and RE male mice. (C) Subtypes of sperm abnormalities in SE and RE male mice. Head abnormalities and compound abnormalities were significantly elevated in the RE group, whereas no significant differences were observed in neck abnormalities or the percentage of immature spermatozoa. (D) Representative photomicrographs of normal and abnormal spermatozoa. (a) Normal spermatozoon; (b) Immature sperm; (c) Head defect; (d) Compound abnormal sperm; (e) Neck defect. Data are presented as mean ± standard deviation (SD). n = 10 mice per group. RE: paternal Wi-Fi RF-EMR exposure group; SE: sham exposure group. Statistical significance was determined by two-sided independent sample *t*-tests (RE vs. SE). ** indicates $p < 0.01$; ns indicates no significant difference ($p > 0.05$).

Table 1
Litter size, placental weight, fetal weight, and placental efficiency.

Variable	SE Group	RE Group	P-value
Litters	10	15	
Litter size	9.7 ± 3.2	7.3 ± 4.0	0.012
Number of male fetuses per litter	4.7 ± 1.3	3.9 ± 2.3	0.481
Number of female fetuses per litter	5 ± 1.9	3.4 ± 1.8	0.103
Male fetal weight (mg)	1425.7 ± 143	1316.9 ± 235	0.004
Male placental weight (mg)	101 ± 16	108 ± 23	0.068
Female fetal weight (mg)	1398.6 ± 211	1268.9 ± 225	0.0047
Female placental weight (mg)	94 ± 15	96 ± 15	0.518
Male placental efficiency	14.21 ± 1.95	12.20 ± 2.20	0.001
Female placental efficiency	14.86 ± 2.11	13.71 ± 2.05	0.0085

Data are expressed as mean ± standard deviation (SD). Statistical comparisons between SE Group and RE Group were performed using independent two-sample *t*-tests. n = 10 litters for SE Group, n = 15 litters for RE Group. P < 0.05 was considered statistically significant.

Table 1, litter size was significantly smaller in the RE group than in the SE group (7.3 ± 4.0 vs. 9.7 ± 3.2, $p = 0.012$). However, no significant differences were observed between the two groups in the numbers of male (3.9 ± 2.3 vs. 4.7 ± 1.3, $p = 0.481$) or female (3.4 ± 1.8 vs. 5.0 ± 1.9, $p = 0.103$) fetuses per litter.

Compared with the SE group, the RE group exhibited significantly lower fetal weights in both male (1316.9 ± 235 mg vs. 1425.7 ± 143 mg, $p = 0.004$) and female (1268.9 ± 225 mg vs. 1398.6 ± 211 mg, $P = 0.0047$) offspring (Table 1). In contrast, placental weights did not differ significantly between the groups for either male (108 ± 23 mg vs. 101 ± 16 mg, $P = 0.068$) or female (96 ± 15 mg vs. 94 ± 15 mg, $P = 0.518$) fetuses (Table 1).

Placental efficiency was significantly reduced following paternal RF-EMR exposure, with a more pronounced reduction observed in male offspring. Specifically, placental efficiency was significantly lower in the RE group than in the SE group for both male (12.20 ± 2.20 vs. 14.21

± 1.95, $p < 0.001$) and female (13.71 ± 2.05 vs. 14.86 ± 2.11, $p = 0.0085$) offspring, although the magnitude of the reduction was greater in males (Table 1). These findings suggest a sex-specific susceptibility to paternal RF-EMR exposure, with male offspring being more vulnerable.

3.3. Sex-dependent alterations in placental structure and gene expression of F1 Progeny

At 18.5 dpc, paternal Wi-Fi RF-EMR exposure induced sex-specific changes in the placental labyrinth layer of F1 offspring. In male offspring, the proportion of the labyrinth layer was significantly reduced in the RE group (49.52% ± 7.88%) compared with the SE group (59.96% ± 2.97%, $p = 0.005$; Fig. 2A-B). In contrast, no significant difference in the proportion of the labyrinth layer was observed between the RE (54.42% ± 6.83%) and SE (57.14% ± 3.05%, $p = 0.327$) groups in female offspring (Fig. 2C-D).

Gene expression profiling of key placental regulatory genes revealed sexually dimorphic responses to paternal RF-EMR exposure. In male placentas, the RE group exhibited significant upregulation of *Gcm1* ($p = 0.013$), *Gbe1* ($p = 0.046$), *Gys1* ($p = 0.023$), *Hand1* ($p = 0.021$), *Pcdh12* ($p = 0.004$), and *Tpbpa* ($p = 0.005$) compared with the SE group (Fig. 2E), whereas no significant differences were observed for *Flk1* or *Gjb3* (both $p > 0.05$). In female offspring placentas, only *Gcm1* ($p = 0.004$) and *Gjb3* ($p = 0.004$) were significantly upregulated in the RE group (Fig. 2E), whereas *Flk1*, *Gbe1*, *Gys1*, *Hand1*, *Pcdh12*, and *Tpbpa* showed no significant differences between the two groups (all $p > 0.05$).

3.4. Unchanged placental microvascular density but dysregulated nutrient transporters in F1 Placentas

Given the close association between placental efficiency and microvascular density within the labyrinth layer, we further examined the effect of paternal RF-EMR exposure on placental vascularization. At 18.5 dpc, microvascular density in the labyrinth layer of F1 placentas did not differ significantly between the RE and SE groups in either sex: male offspring (RE: 707.56 ± 86.15 vs. SE: 713.29 ± 76.82, $p = 0.741$) (Fig. 3A-B) and female offspring (RE: 693.02 ± 75.26 vs. SE: 704.67 ± 50.43, $p = 0.723$) (Fig. 3C-D).

Because placental efficiency is closely associated with nutrient transporter expression, we next examined the expression of 12 key nutrient transporter genes in F1 placentas, including Na^+/K^+-ATPase

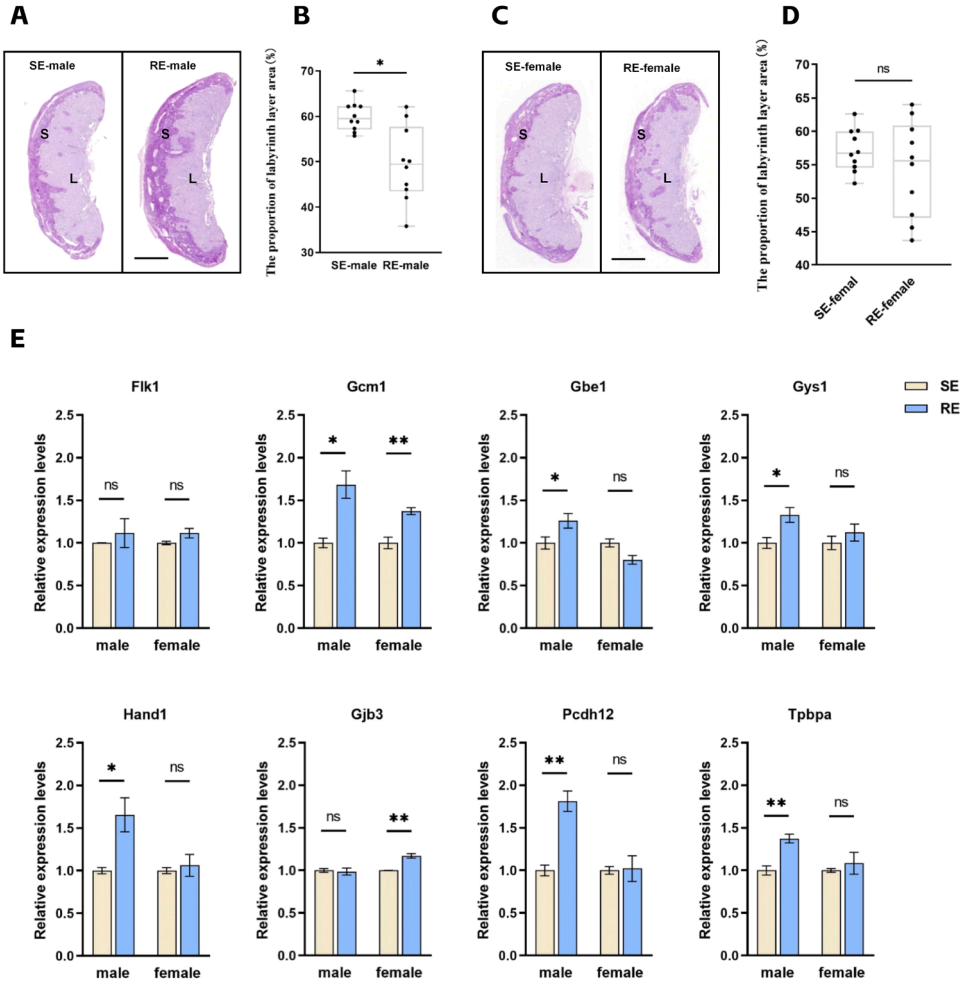

Fig. 2. Histological and molecular analysis of placental structure and gene expression. (A) PAS staining of placentas from male offspring in the SE and RE groups. Red-stained regions represent the spongiotrophoblast layer, while light red areas indicate the labyrinth zone. Scale bars: 1 mm. (B) Quantitative comparison of the labyrinth layer-to-total placental area ratio in male offspring between the SE and RE groups. (C) PAS staining of placentas from female offspring in the SE and RE groups. Scale bars: 1 mm. (D) Labyrinth layer-to-total placental area ratio in female offspring of the SE and RE groups. (E) Relative mRNA expression levels of key placental developmental genes at embryonic day 18.5 (E18.5). Data are presented as mean ± standard deviation (SD). For PAS staining and morphometric analysis (A–D), n = 10 placentas per group. For RT-qPCR (E), n = 6 placentas from 3 independent dams per group. Statistical significance was determined by two-sided independent sample *t*-tests (RE vs. SE within the same sex). * Indicates $p < 0.05$; ** indicates $p < 0.01$; ns indicates no significant difference ($p > 0.05$). RE: paternal Wi-Fi RF-EMR exposure group; SE: sham exposure group.

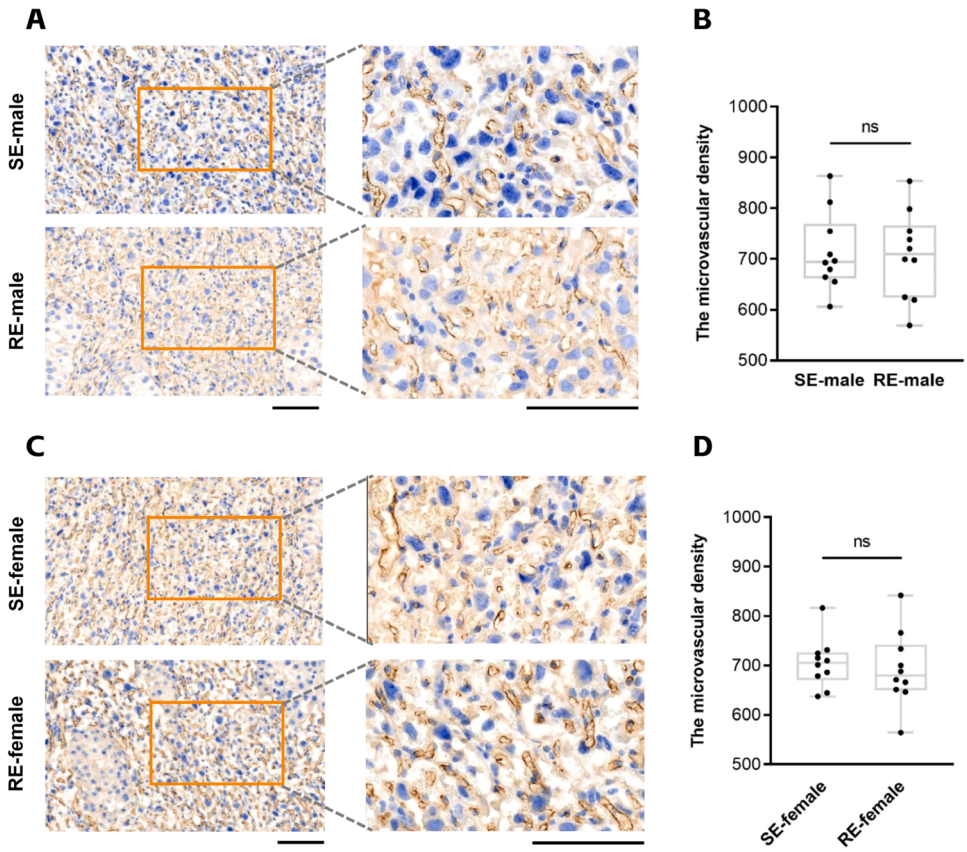

Fig. 3. Microvascular immunohistochemical analysis of placentas in SE and RE groups. (A) Representative CD31 immunostaining images showing microvessel density (MVD) in placental tissues from male offspring of the SE and RE groups. Scale bars: 100 μm. (B) Quantitative analysis of MVD in male offspring placentas. (C) Representative CD31 immunostaining images showing MVD in placental tissues from female offspring of the SE and RE groups. Scale bars: 100 μm. (D) Quantitative analysis of MVD in female offspring placentas. Data are presented as mean ± standard deviation (SD). n = 6 placentas from 3 independent dams per group. Statistical significance was determined by two-sided independent sample *t*-tests (RE vs. SE within the same sex). *ns* indicates no significant difference ($p > 0.05$). RE: paternal Wi-Fi RF-EMR exposure group; SE: sham exposure group.

subunits (*Atp1a1* and *Atp2a3*); glucose transporters (*Slc2a1* and *Slc2a3*); the solute carrier family 3 member 2 (*Slc3a2*); the taurine transporter (*Slc6a6*); the thiamine transporter (*Slc19a2*); an organic ion transporter (*Slc22a3*); System A amino acid transporters (*Slc38a1, Slc38a2*, and *Slc38a4*); and the iron transporter (*Slc40a1*).

In male offspring placentas, seven transporter genes (*Atp1a1*, $p = 0.027$; *Atp2a3*, $p = 0.021$; *Slc2a1*, $p = 0.032$; *Slc2a3*, $p = 0.013$; *Slc3a2*, $p = 0.047$; *Slc22a3*, $p = 0.038$; *Slc40a1*, $p = 0.039$) were significantly downregulated in the RE group, whereas the remaining five (*Slc6a6*, *Slc19a2*, *Slc38a1*, *Slc38a2*, and *Slc38a4*) showed no significant differences (all $p > 0.05$) (Fig. 4). In female offspring placentas, only three transporter genes (*Slc2a3*, $p = 0.026$; *Slc38a1*, $p = 0.048$; and *Slc40a1*, $p = 0.009$) were significantly downregulated in the RE group (Fig. 4), while the other nine (*Atp1a1*, *Atp2a3*, *Slc2a1*, *Slc3a2*, *Slc6a6*, *Slc19a2*, *Slc22a3*, *Slc38a2*, and *Slc38a4*) showed no significant differences (all $p > 0.05$) (Fig. 4).

3.5. Paternal RF-EMR induces sex-specific histone modification dysregulation in F1 placentas

Histone modifications play a critical role in the precise regulation of gene expression (Fowden et al., 2009). Compared with placentas from the same-sex SE group, male placentas in the RE group exhibited significantly increased levels of H3K27ac ($p = 0.009$), H3K27me3 ($p < 0.001$), H3K9me3 ($p = 0.003$), H3K9me2 ($p = 0.006$), and H3K4me2 ($p = 0.002$), whereas H3K4me3 levels did not differ significantly ($p > 0.05$) (Fig. 5A-B). In contrast, female placentas in the RE group exhibited only a significant reduction in H3K4me2 levels ($p < 0.001$), with no significant differences in the other histone modifications (all $p > 0.05$) (Fig. 5C-D).

3.6. Sex-specific histone modification changes are associated with downregulation of nutrient transporter expression in placentas

To determine whether the repressive histone marks H3K27me3 and H3K9me3 contribute to the sex-specific downregulation of placental nutrient transporters, we performed ChIP-qPCR on placental tissues from both sexes, focusing on the promoter regions of the five genes (*Atp1a1*, *Atp2a3*, *Slc2a1*, *Slc3a2*, and *Slc22a3*) that were significantly downregulated exclusively in male placentas. The results revealed a distinct sex-dependent pattern of repressive histone mark enrichment. In male placentas from the RE group, H3K27me3 occupancy was significantly increased at the *Atp1a1* ($p = 0.0258$) and *Slc22a3* ($p = 0.0125$) promoters compared with the SE group, whereas no significant differences were detected at the *Atp2a3* ($p = 0.2309$), *Slc2a1* ($p = 0.0916$), or *Slc3a2* ($p = 0.338$) promoters (Fig. 6A). Similarly, H3K9me3 enrichment was significantly increased at the *Atp1a1* ($p < 0.001$) and *Slc2a1* ($p = 0.0067$) promoters in male placentas from the RE group but remained unchanged at the *Atp2a3* ($p = 0.8559$), *Slc3a2* ($p = 0.795$), and *Slc22a3* ($p = 0.4987$) promoters (Fig. 6B). In marked contrast, female placentas from the RE group exhibited only one significant alteration: decreased H3K27me3 enrichment at the *Slc3a2* promoter ($p = 0.0356$), with no significant enrichment of either repressive histone mark at any of the other promoters examined (all $p > 0.05$) (Fig. 6C-D). These findings demonstrate a male-specific association between repressive histone modifications and the transcriptional suppression of

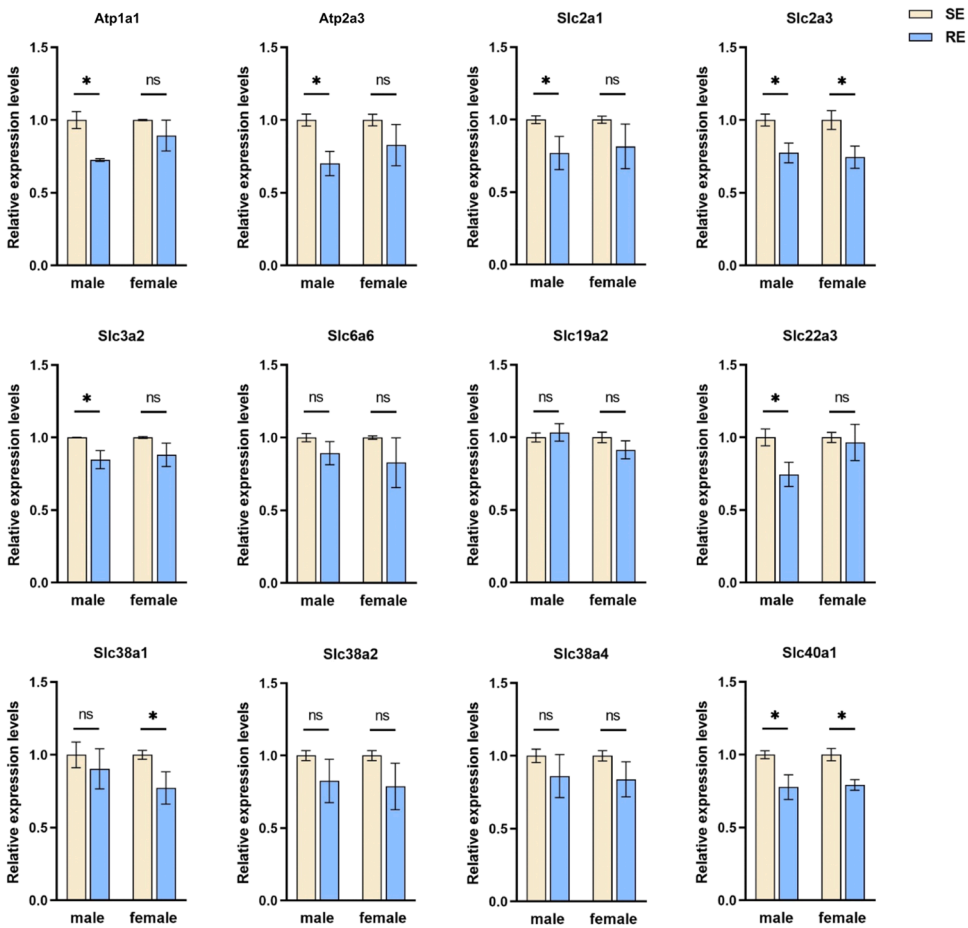

Fig. 4. Expression profiles of placental nutrient transporter genes in SE and RE groups at E18.5. Cation transporters: Na^+/K^+-ATPase subunits (*Atp1a1*, *Atp2a3*); Glucose transporters: *Slc2a1*and *Slc2a3*; Amino acid transporters: *Slc3a2*, *Slc38a1*, *Slc38a2* and *Slc38a4*; Specialized transporters: taurine (*Slc6a6*), thiamine (*Slc19a2*), organic ion/iron *(Slc22a3*, *Slc40a1*). Data are presented as mean ± SD. n = 6 placentas from 3 independent dams per group. Statistical significance was determined by two-sided independent sample *t*-tests (RE vs. SE within the same sex). * indicates $p < 0.05$; ** indicates $p < 0.01$; ns indicates no significant difference ($p > 0.05$). RE: paternal Wi-Fi RF-EMR exposure group; SE: sham exposure group.

placental nutrient transporters following paternal RF-EMR exposure.

4. Discussion

The rapid advancement and widespread adoption of wireless communication technologies have substantially increased personal exposure to radiofrequency electromagnetic fields (RF-EMF). Consequently, public concern has grown regarding the potential adverse health effects associated with Wi-Fi-derived RF-EMR exposure. Numerous studies have shown that Wi-Fi-derived RF-EMR may impair male fertility, as evidenced by abnormal testicular histology, altered sex hormone levels, and reduced sperm motility. However, the intergenerational health risks associated with paternal exposure remain poorly understood. According to the International Commission on Non-Ionizing Radiation Protection (ICNIRP), the whole-body exposure limits, expressed as the specific absorption rate (SAR), are 0.08 W/kg for the general population and 0.4 W/kg for occupational exposure (International Commission on Non-Ionizing Radiation, 2020). In the present study, the estimated whole-body SAR ranged from 0.125 to 0.5 W/kg. Importantly, because of allometric differences in metabolism, the same SAR imposes a greater physiological burden in mice than in humans. Using this exposure paradigm, we demonstrated that chronic paternal Wi-Fi RF-EMR exposure in mice reduced fetal weight and impaired placental efficiency in the offspring. Notably, we identified a sex-specific effect in this murine model, with male offspring exhibiting more pronounced placental impairments than female offspring, indicating a male-biased susceptibility to paternal RF-EMR exposure. Given the greater physiological impact of the applied SAR in mice, these findings cannot be directly extrapolated to humans at equivalent SAR levels. Nevertheless, potential intergenerational risks cannot be excluded, particularly among occupationally exposed populations whose SAR levels may approach those used in the present study. Therefore, our findings do not warrant public alarm but support the consideration of preconception health recommendations for occupationally exposed men and suggest that regulatory agencies re-evaluate whether current exposure limits, which are primarily based on thermal effects, adequately account for potential non-thermal, epigenetic, and sex-specific outcomes.

Both clinical and animal studies have demonstrated that exposure to Wi-Fi-derived RF-EMR reduces sperm viability and motility while increasing the incidence of morphological abnormalities (Vijay et al., 2025; Avendano et al., 2012; Maluin et al., 2024). Our findings are consistent with these reports. In the present study, prolonged RF-EMR exposure significantly reduced epididymal sperm concentration and increased the frequency of sperm morphological abnormalities in male mice, particularly head abnormalities and compound abnormalities. Additionally, we evaluated the proportion of immature spermatozoa but found no significant difference between the exposed and control groups.

Several epidemiological and experimental studies have specifically examined the effects of paternal RF-EMR exposure on offspring health. Epidemiological studies have linked paternal occupational RF-EMR exposure to an increased risk of preterm birth, certain congenital

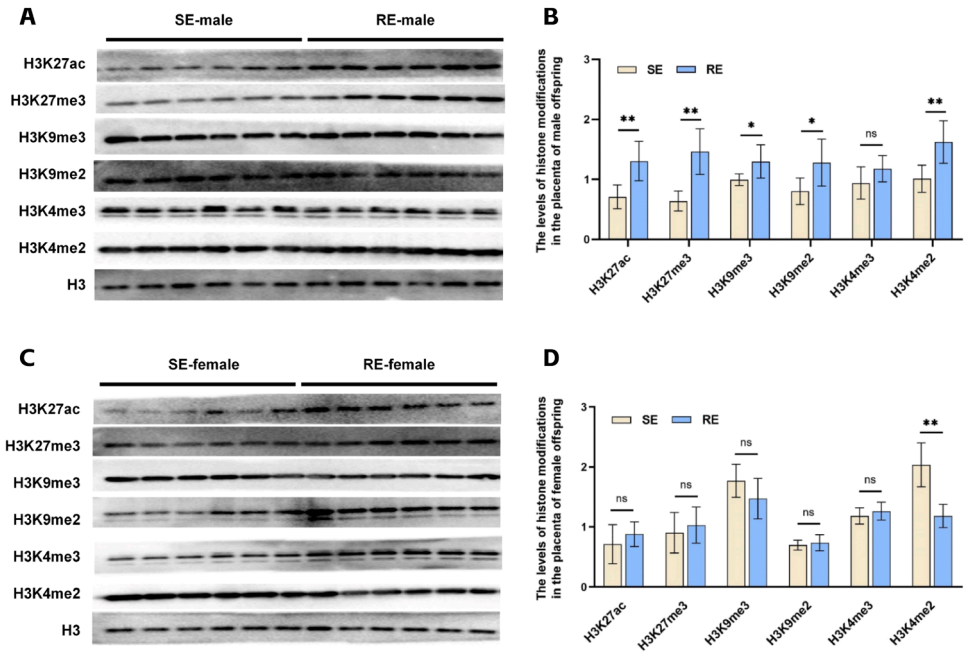

Fig. 5. Histone modification levels in the placenta of offspring from SE and RE groups. (A) Representative Western blot images of histone modifications (H3K27ac, H3K27me3, H3K9me3, H3K9me2, H3K4me3, H3K4me2, and total H3) in the placenta of male offspring from SE and RE groups. (B) Quantitative analysis of histone modification levels in the placenta of male offspring. (C) Representative Western blot images of histone modifications in the placenta of female offspring from SE and RE groups. (D) Quantitative analysis of histone modification levels in the placenta of female offspring. Data are presented as mean ± SD. n = 6 placentas from 3 independent dams per group. Statistical significance was determined by two-sided independent sample *t*-tests (RE vs. SE within the same sex). * indicates $p < 0.05$; ** indicates $p < 0.01$; ns indicates no significant difference ($p > 0.05$). RE: paternal Wi-Fi RF-EMR exposure group; SE: sham exposure group.

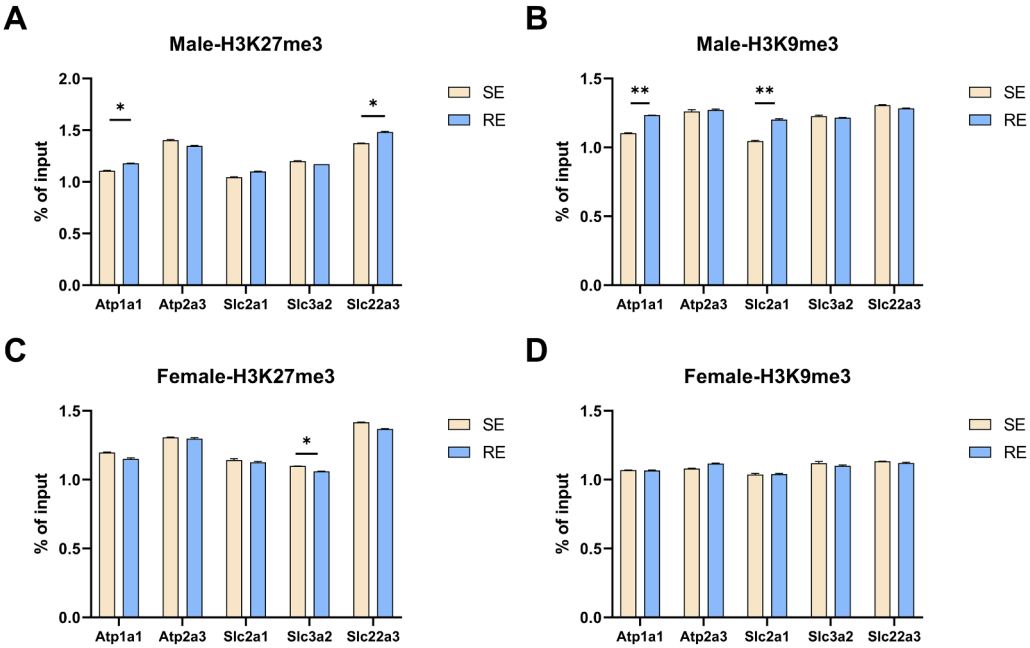

Fig. 6. Sex-specific enrichment of repressive histone marks at nutrient transporter promoters in F1 placentas. ChIP-qPCR analysis of H3K27me3 (A, C) and H3K9me3 (B, D) enrichment at the promoter regions of nutrient transporter genes (*Atp1a1*, *Atp2a3*, *Slc2a1*, *Slc3a2*, and *Slc22a3*) in male (A, B) and female (C, D) placentas at E18.5. Data are presented as mean ± SD (n = 6 placentas from 3 independent dams per group). Statistical significance was determined by two-sided independent sample *t*-tests (RE vs. SE within the same sex). * indicates $p < 0.05$; ** indicates $p < 0.01$; ns indicates no significant difference ($p > 0.05$). E: paternal Wi-Fi RF-EMR exposure group; SE: sham exposure group.

anomalies, and a higher incidence of neuroblastoma in offspring (Baste et al., 2008; Mjoen et al., 2006; Blaasaas et al., 2002). In animal models, paternal exposure to 900 MHz GSM-like radiation in Xenopus laevis resulted in increased embryonic mortality and morphological abnormalities, particularly when both parents were exposed (Boga et al., 2016). In zebrafish, Wi-Fi RF-EMR exposure in adults impaired reproduction and induced intergenerational morphological and behavioral abnormalities in the offspring (Mehta et al., 2025). In rodents, paternal

exposure to mobile phone radiation reduced litter size and birth weight (Kesari and Behari, 2012). Our previous study demonstrated that paternal RF-EMR exposure induces sex-specific alterations in body weight trajectories and glucose metabolism in mouse offspring (Yan et al., 2022). Based on these findings, we hypothesized that paternal RF-EMR exposure may exert intergenerational effects through sperm-mediated mechanisms. To test this hypothesis, we evaluated the effects of chronic paternal Wi-Fi-derived RF-EMR exposure on fetal intrauterine growth and placental efficiency. Compared with the SE group, the RE group exhibited significantly lower fetal weights in both male and female offspring. Because fetal growth largely depends on placental nutrient supply, we evaluated placental efficiency, defined as fetal weight per unit placental weight, as a key indicator of placental nutrient transfer capacity (Fowden et al., 2009; Sun et al., 2020). Notably, chronic paternal RF-EMR exposure significantly reduced placental efficiency in offspring of both sexes; however, the reduction was substantially greater in male offspring than in female offspring, indicating a male-biased susceptibility to paternal RF-EMR exposure. This sex-dependent reduction in placental functional efficiency was consistent with the observed structural changes, as male placentas exhibited a significant decrease in the proportion of the labyrinth layer, whereas no such change was observed in female placentas. We further investigated the effects of paternal Wi-Fi RF-EMR exposure on placental gene expression. In male placentas from the exposed group, the spongiotrophoblast/glycogen cell marker *Tpbpa*, the glycogen metabolism-related genes (*Gys1* and *Gbe1*), the trophoblast giant cell differentiation factor *Hand1*, and the vascularization regulator *Pcdh12* were all significantly upregulated, consistent with the observed morphological alterations (Chen et al., 2015; Hasan et al., 2015; Rampon et al., 2008). The syncytiotrophoblast marker *Gcm1* was upregulated in placentas of both sexes, suggesting compromised labyrinthine integrity (Chen et al., 2015). These findings indicate sex-specific dysregulation of placental developmental genes following paternal RF-EMR exposure. Collectively, our results provide the first evidence that the reduction in fetal weight induced by chronic paternal Wi-Fi RF-EMR exposure is associated with placental dysfunction. Furthermore, we demonstrate for the first time that chronic paternal Wi-Fi RF-EMR exposure induces sex-specific alterations in placental labyrinth layer proportion and disrupts the expression of placental developmental genes, with male offspring exhibiting greater susceptibility.

Placental efficiency in mice is primarily determined by labyrinthine vascular density and the expression of nutrient transporters (Angiolini et al., 2006; Audette et al., 2018). However, analysis of placental microvascular density indicated that paternal Wi-Fi-derived RF-EMR exposure did not affect placental vascularization in offspring of either sex. To further elucidate the mechanisms underlying these sex-dependent effects, we investigated the influence of paternal Wi-Fi-derived RF-EMR exposure on the expression of placental nutrient transporters. Quantitative analysis of 12 key nutrient transporter genes revealed extensive downregulation in male placentas from the paternal exposure group, with seven transporters being significantly affected. These included the Na^+/K^+-ATPase subunits (*Atp1a1* and *Atp2a3*), the glucose transporters *Slc2a1* and *Slc2a3*, the amino acid transporter *Slc3a2*, and the organic ion and iron transporters *Slc22a3* and *Slc40a1*. In contrast, female placentas from the paternal exposure group exhibited significant downregulation of only three transporters: *Slc2a3*, *Slc38a1*, and *Slc40a1*. At the molecular level, these findings further support a male-specific susceptibility to paternal Wi-Fi RF-EMR exposure, characterized by widespread downregulation of placental nutrient transporter expression in male offspring, whereas female offspring exhibited only limited changes. This sexually dimorphic pattern of transporter dysregulation directly links paternal RF-EMR exposure to impaired placental nutrient transport capacity, providing a mechanistic explanation for the more pronounced impairment in fetal growth observed in male offspring.

Histone modifications are critical regulators of developmental gene expression (Millan-Zambrano et al., 2022). Among these, H3K27ac marks active chromatin states (Sabari et al., 2017), whereas H3K27me3 and H3K9me2/3 are repressive marks associated with gene silencing (Macrae et al., 2023), and H3K4me2 plays a dual role in transcriptional regulation (Macrae et al., 2023). In the present study, paternal Wi-Fi RF-EMR exposure induced sex-dependent histone modification profiles in F1 placentas: male placentas exhibited significant increases in H3K27ac, H3K27me3, H3K9me2, H3K9me3, and H3K4me2, whereas female placentas exhibited only a global decrease in H3K4me2. To investigate whether these global epigenetic alterations directly affect placental nutrient transporter expression, ChIP-qPCR was performed targeting the promoter regions of the five transporters that were downregulated exclusively in male placentas (*Atp1a1*, *Atp2a3*, *Slc2a1*, *Slc3a2*, and *Slc22a3*). This analysis revealed a sex-specific pattern of repressive histone mark enrichment. In male placentas from the exposed group, H3K27me3 occupancy was significantly increased at the *Atp1a1* and *Slc22a3* promoters, whereas H3K9me3 enrichment was elevated at the *Atp1a1* and *Slc2a1* promoters. In contrast, female placentas exhibited only one significant change—decreased H3K27me3 enrichment at the *Slc3a2* promoter. This promoter-specific, male-restricted accumulation of repressive histone marks provides a direct mechanistic link between paternal RF-EMR exposure and transcriptional suppression of placental nutrient transporters, a link that is not observed in female placentas and that underscores male-biased epigenetic susceptibility to paternal environmental exposure.

Paternal RF-EMR exposure induced sex-specific histone modifications in F1 placentas, raising the critical question of how these epigenetic alterations are transmitted across generations. Sperm carry multiple layers of epigenetic information, including DNA methylation, histone retention, and non-coding RNAs (ncRNAs), all of which have been proposed as potential mediators of intergenerational inheritance (Liao et al., 2025). However, following fertilization, the zygote undergoes extensive epigenetic reprogramming, during which most sperm-derived DNA methylation patterns and chromatin modifications are globally erased and subsequently re-established, thereby substantially limiting their potential for direct transmission (Xavier et al., 2019; Burton and Torres-Padilla, 2025). In contrast, sperm-borne ncRNAs—including small RNAs (miRNAs, piRNAs, and tsRNAs) as well as long non-coding RNAs—can largely evade this reprogramming process and regulate early embryonic gene expression, making them the most plausible carriers of paternally acquired environmental information (Liao et al., 2025; Tomar et al., 2024; Wu et al., 2025).

Consistent with this hypothesis, accumulating evidence indicates that sperm-borne ncRNAs play a central role in mediating paternal environmental effects on offspring development. A variety of paternal exposures have been shown to remodel the sperm ncRNA repertoire, thereby influencing offspring metabolic homeostasis (Hernandez et al., 2024; Park et al., 2026; Argaw-Denboba et al., 2024). Furthermore, sperm-derived ncRNAs have been implicated in early placental lineage specification and the regulation of placental function (Jodar, 2019; de la Iglesia et al., 2026), providing a biologically plausible mechanism linking paternal RF-EMR exposure to the sex-specific placental phenotypes observed in the present study.

Nevertheless, the molecular mechanisms by which RF-EMR alters the sperm ncRNA landscape remain largely unclear. Because RF-EMR is a well-recognized inducer of oxidative stress (Houston et al., 2016; Shokri et al., 2020), and oxidative stress has been shown to profoundly reshape the sperm small non-coding RNA (sncRNA) profile (Ren et al., 2022; Moazamian et al., 2025), we propose that chronic Wi-Fi exposure may remodel the sperm ncRNA repertoire in F0 males through oxidative stress-dependent pathways. Notably, the epididymis is likely the primary site where these alterations occur. In contrast to developing germ cells within the testis, which are protected by the blood–testis barrier, spermatozoa traversing the epididymis are directly exposed to luminal fluids and extracellular vesicles enriched in somatic cell-derived ncRNAs, thereby undergoing extensive post-testicular RNA remodeling

(Trigg and Conine, 2024; Conine et al., 2018). Importantly, compelling evidence indicates that sperm-borne ncRNAs—particularly those acquired during epididymal transit—play critical regulatory roles in early embryonic development and placental function (Trigg and Conine, 2024; Conine et al., 2018; Warkiani and Goss, 2026). This unique maturation window thus renders epididymal sperm and their acquired ncRNA cargo particularly vulnerable to oxidative stress and environmental perturbations.

Despite these observations, direct evidence demonstrating that RF-EMR-induced alterations in sperm ncRNAs causally drive the sex-specific histone reprogramming observed in F1 placentas is still lacking. Future studies should systematically characterize both small RNAs and long non-coding RNAs in epididymal sperm following RF-EMR exposure and determine their functional significance using embryo microinjection or *in vitro* fertilization models combined with RNA depletion and rescue strategies. Such investigations will provide critical mechanistic insights into how paternal RF-EMR exposure is epigenetically transmitted to the placenta and may ultimately influence offspring development.

Unlike previous studies that primarily focused on direct testicular toxicity or hormonal disruption following RF-EMR exposure, the present study provides the first mammalian evidence that chronic (20-week) paternal Wi-Fi exposure impairs fetal growth through a placenta-mediated mechanism. Moreover, while intergenerational effects have been reported in zebrafish and *Drosophila*, our work demonstrates that long-term paternal Wi-Fi RF-EMR exposure leads to a male-biased susceptibility in placental efficiency and nutrient transporter expression, accompanied by sex-dependent histone modification patterns in the placenta—an area that has received limited attention in previous research on chronic paternal Wi-Fi exposure. However, several limitations of this study should be acknowledged. First, we did not profile the F0 sperm epigenome, including DNA methylation, histone retention, or small non-coding RNAs, which are known carriers of paternally acquired environmental information. Second, the present study assessed fetal and placental outcomes only at 18.5 dpc, thereby missing dynamic changes during early and mid-gestation; longitudinal studies covering multiple developmental windows are therefore needed.

5. Conclusion

This study demonstrates that chronic paternal exposure to Wi-Fi-derived RF-EMR (2.4 GHz, whole-body SAR 0.125–0.5 W/kg, 20 weeks) impairs sperm quality in F0 male mice and adversely affects fetal growth and placental efficiency in F1 offspring in a sex-dependent manner, with male progeny exhibiting significantly greater susceptibility. Specifically, male offspring showed more pronounced reductions in placental efficiency and labyrinth layer proportion, accompanied by broader downregulation of nutrient transporters. Concordantly, paternal RF-EMR exposure induced extensive sex-specific alterations in placental histone modifications in males—elevated H3K27ac, H3K27me3, H3K9me2/3, and H3K4me2—whereas female placentas exhibited only decreased H3K4me2. Mechanistically, ChIP-qPCR revealed a sex-specific enrichment of repressive histone marks at transporter promoters: compared with the sham-exposed group, male placentas from the paternal RF-EMR exposure group displayed increased H3K27me3 occupancy at *Atp1a1* and *Slc22a3*, and elevated H3K9me3 at *Atp1a1* and *Slc2a1*, whereas female placentas showed only decreased H3K27me3 at *Slc3a2*. Collectively, these findings indicate that male offspring are more vulnerable to adverse intrauterine programming following chronic paternal Wi-Fi RF-EMR exposure, and that sex-dependent epigenetic dysregulation—particularly at the level of placental histone modifications and nutrient transporter expression—likely contributes to the male-biased impairments in fetal development. This study highlights the importance of incorporating offspring sex as a key biological variable in reproductive risk assessments of paternal RF-EMR exposure and raises important considerations for preconception health guidance in occupationally exposed populations.

CRediT authorship contribution statement

Ni Jin: Visualization, Methodology. **Lingxia Gao:** Visualization, Methodology, Data curation. **Hui Lei:** Visualization. **Ying Ju:** Visualization, Methodology. **Jun Wang:** Writing – original draft, Visualization, Methodology, Investigation, Data curation. **Shuqiang Chen:** Writing – review & editing, Supervision. **Song Yan:** Visualization. **Xiaohong Wang:** Resources, Funding acquisition, Conceptualization.

Declaration of Competing Interest

The authors declare that there is no conflict of interest that could be perceived as prejudicing the impartiality of the research reported.

Acknowledgments

We are grateful to the other members of our laboratory for their valuable comments. All authors have read and approved the final manuscript. This study was supported by the National Natural Science Foundation of China (Grant No. 82271734).

Appendix Tables 1. . Primer sequences used for RT-qPCR analysis of placental transporter genes

Gene	Primer sequences	
	Forward (5′→3′)	Reverse (5′→3′)
Atp1a1	CAGGCTCCAAGTCCAGTAACC	GGGAGTGGGTGTGATTGACA
Atp2a3	GGAGCAGTTTGAGGACCTCTT	GGCCACGAGAATTAGCATGATG
Slc2a1	GCTTATGGGCTTCTCCAAACT	GGTGACACCTCTCCCACATAC
Slc2a3	GATCGGCTCTTTCCAGTTTG	CAATCATGCCACCAACAGAG
Slc3a2	TGATGAATGCACCCTTGTACTTG	GCTCCCCAGTGAAAGTGGA
Slc6a6	GCACACGGCCTGAAGATGA	ATTTTTGTAGCAGAGGTACGGG
Slc19a2	GTGGCATCGTTACTGATACCC	TTCCACCGGAGGCTCATCTAA
Slc22a3	CTATGCAGCGGACAGATATGG	AGCGGAAAATCACAAACACAGAA
Slc38a1	CCTTCACAAGTACCAGAGCAC	GGCCAGCTCAAATAACGATGAT
Slc38a2	TAATCTGAGCAATGCGATTGTGG	AGATGGACGGAGTATAGCGAAAA
Slc38a4	GCGGGGACAGTATTCAGGAC	GGAACTTCTGACTTTCGGCAT
Slc40a1	ACCAAGGCAAGAGATCAAACC	AGACACTGCAAAGTGCCACAT
Gapdh	TGACATCAAGAAGGTGGTGAAG	AGAGTGGGAGTTGCTGTTGAAG

Appendix Tables 2. . Primer sequences used for RT-qPCR analysis of placental marker genes

Gene	Primer sequences	
	Forward (5′→3′)	Reverse (5′→3′)
Flk1	GGCGGTGGTGACAGTATCTT	GTCACTGACAGAGGCGATGA
Gcm1	AGCCTGTGTTGAGCAGACCT	TGTCGTCCGAGCTGTAGATG
Gbe1	GGACGCTGAGATGTACACGA	AGTCCAACCATTCAGGATGC
Gys1	GGAGAAATTTGGGAGGAAGC	GTCAAGATGGGGTCTGAGGA
Hand1	CGCCTGGCTACCAGTTACAT	GCGCCCTTTAATCCTCTTCT
Gjb3	GGGGCTCTCCATCAGACATA	ACCTGCTAGCCACACTTGCT
Pcdh12	AAGCAGAACCTGACCTGGAA	GTGAGGGGCAATGACAATCT
Tpbpa	TGAAGAGCTGAACCACTGGA	CTTGCAGTTCAGCATCCAAC

Appendix Tables 3. . Primer sequences used for ChIP-qPCR analysis

Gene	Primer sequences	
	Forward (5′→3′)	Reverse (5′→3′)
Atp1a1	AGTAGACTAGCCCCGACTGC	GGTGTCTGGGTCTCTCAAGG
Atp2a3	TTTCTTCCGCAAGAGACCCC	CAAAGCTGGGGGACCTACTG
Slc2a1	ACCAAGCGCTACCATTTTGC	CTCTGAGAGGCGTGGTTCTG
Slc3a2	TAAGCCCCGAGGAGAATCCA	CAGGTTTCAAAGCCCCTCCT
Slc22a3	AGGTGAGGACCGGAAGAAGA	GCATGTGTGGTCCCTATCGT

Data availability

Data will be made available on request.

References

Abtin, S., Seyedaghamiri, F., Aalidaeijavadi, Z., Farrokhi, A.M., Moshrefi, F., Ziveh, T., Zibaii, M.I., Aliakbarian, H., Rezaei-Tavirani, M., Haghparast, A., 2024. A review on the consequences of molecular and genomic alterations following exposure to electromagnetic fields: Remodeling of neuronal network and cognitive changes. Brain Res. Bull. 217, 111090.

Ali, A., Mistry, B.V., Ahmed, H.A., Abdulla, R., Amer, H.A., Prince, A., Alazami, A.M., Alkuraya, F.S., Assiri, A., 2018. Deletion of DDB1- and CUL4- associated factor-17 (Dcaf17) gene causes spermatogenesis defects and male infertility in mice. Sci. Rep. 8 (1), 9202.

Angiolini, E., Fowden, A., Coan, P., Sandovici, I., Smith, P., Dean, W., Burton, G., Tycko, B., Reik, W., Sibley, C., Constancia, M., 2006. Regulation of placental efficiency for nutrient transport by imprinted genes (Suppl A). Placenta 27, S98.

Argaw-Denboba, A., Schmidt, T.S.B., Di Giacomo, M., Ranjan, B., Devendran, S., Mastrorilli, E., Lloyd, C.T., Pugliese, D., Paribeni, V., Dabin, J., Pisaniello, A., Espinola, S., Crevenna, A., Ghosh, S., Humphreys, N., Boruc, O., Sarkies, P., Zimmermann, M., Bork, P., Hackett, J.A., 2024. Paternal microbiome perturbations impact offspring fitness. Nature 629 (8012), 652–659.

Ashapkin, V., Suvorov, A., Pilsner, J.R., Krawetz, S.A., Sergeyev, O., 2023. Age-associated epigenetic changes in mammalian sperm: implications for offspring health and development. Hum. Reprod. Update 29 (1), 24–44.

Audette, M.C., Levytska, K., Lye, S.J., Melamed, N., Kingdom, J.C., 2018. Parental ethnicity and placental maternal vascular malperfusion pathology in healthy nulliparous women. Placenta 66, 40–46.

Avendano, C., Mata, A., Sanchez Sarmiento, C.A., Doncel, G.F., 2012. Use of laptop computers connected to internet through Wi-Fi decreases human sperm motility and increases sperm DNA fragmentation. Fertil. Steril. 97 (1), 39–45 e2.

Baste, V., Riise, T., Moen, B.E., 2008. Radiofrequency electromagnetic fields; male infertility and sex ratio of offspring. Eur. J. Epidemiol. 23 (5), 369–377.

Baste, V., Moen, B.E., Oftedal, G., Strand, L.A., Bjorge, L., Mild, K.H., 2012. Pregnancy outcomes after paternal radiofrequency field exposure aboard fast patrol boats. J. Occup. Environ. Med. 54 (4), 431–438.

Bektas, H., Dasdag, S., 2025. The effects of radiofrequency radiation on male reproductive health and potential mechanisms. Electromagn. Biol. Med. 44 (3), 359–384.

Blaasaas, K.G., Tynes, T., Irgens, A., Lie, R.T., 2002. Risk of birth defects by parental occupational exposure to 50 Hz electromagnetic fields: a population based study. Occup. Environ. Med. 59 (2), 92–97.

Boga, A., Emre, M., Sertdemir, Y., Uncu, I., Binokay, S., Demirhan, O., 2016. Effects of GSM-like radiofrequency irradiation during the oogenesis and spermiogenesis of Xenopus laevis. Ecotoxicol. Environ. Saf. 129, 137–144.

Burton, A., Torres-Padilla, M.E., 2025. Epigenome dynamics in early mammalian embryogenesis. Nat. Rev. Genet. 26 (9), 587–603.

Cakmak, E., Bilgici, B., Engiz, B.K., Kocaman, A., 2026. Effects of wireless local area network exposure on testicular morphology and VEGF levels. Sci. Rep. 16 (1), 6387.

Cantu, J.C., Butterworth, J.W., Peralta, X.G., Payne, J.A., Echchgadda, I., 2023. Analysis of global DNA methylation changes in human keratinocytes immediately following exposure to a 900 MHz radiofrequency field. Bioelectromagnetics 44 (3-4), 77–89.

Cappucci, U., Casale, A.M., Proietti, M., Marinelli, F., Giuliani, L., Piacentini, L., 2022. WiFi Related Radiofrequency Electromagnetic Fields Promote Transposable Element Dysregulation and Genomic Instability in Drosophila melanogaster. Cells 11 (24).

Chen, S., Sun, F.Z., Huang, X., Wang, X., Tang, N., Zhu, B., Li, B., 2015. Assisted reproduction causes placental maldevelopment and dysfunction linked to reduced fetal weight in mice. Sci. Rep. 5, 10596.

Conine, C.C., Sun, F., Song, L., Rivera-Perez, J.A., Rando, O.J., 2018. Small RNAs Gained during Epididymal Transit of Sperm Are Essential for Embryonic Development in Mice. Dev. Cell. 46 (4), 470–480 e3.

Dasdag, S., Akdag, M.Z., Erdal, M.E., Erdal, N., Ay, O.I., Ay, M.E., Yilmaz, S.G., Tasdelen, B., Yegin, K., 2015b. Effects of 2.4 GHz radiofrequency radiation emitted from Wi-Fi equipment on microRNA expression in brain tissue. Int. J. Radiat. Biol. 91 (7), 555–561.

Dasdag, S., Tas, M., Akdag, M.Z., Yegin, K., 2015a. Effect of long-term exposure of 2.4 GHz radiofrequency radiation emitted from Wi-Fi equipment on testes functions. Electromagn. Biol. Med. 34 (1), 37–42.

Dasdag, S., Akdag, M.Z., Erdal, M.E., Erdal, N., Ay, O.I., Ay, M.E., Yilmaz, S.G., Tasdelen, B., Yegin, K., 2015c. Long term and excessive use of 900 MHz radiofrequency radiation alter microRNA expression in brain. Int. J. Radiat. Biol. 91 (4), 306–311.

de la Iglesia, A., Prip-Buus, C., Maillard, G.L., Vaiman, D., Cocquet, J., 2026. Uneven impacts: how male diet modulates the sperm epigenome and impacts embryo development and pregnancy healthdagger. Biol. Reprod. 114 (2), 375–395.

De Roos, A.J., Teschke, K., Savitz, D.A., Poole, C., Grufferman, S., Pollock, B.H., Olshan, A.F., 2001. Parental occupational exposures to electromagnetic fields and radiation and the incidence of neuroblastoma in offspring. Epidemiology 12 (5), 508–517.

Ding, S.S., Sun, P., Zhang, Z., Liu, X., Tian, H., Huo, Y.W., Wang, L.R., Han, Y., Xing, J.P., 2018. Moderate Dose of Trolox Preventing the Deleterious Effects of Wi-Fi Radiation on Spermatozoa In vitro through Reduction of Oxidative Stress Damage. Chin. Med. J. (Engl.) 131 (4), 402–412.

Fowden, A.L., Sferruzzi-Perri, A.N., Coan, P.M., Constancia, M., Burton, G.J., 2009. Placental efficiency and adaptation: endocrine regulation. J. Physiol. 587 (Pt 14), 3459–3472.

Giorgi, G., Del Re, B., 2021. Epigenetic dysregulation in various types of cells exposed to extremely low-frequency magnetic fields. Cell. Tissue Res. 386 (1), 1–15.

Hasan, M.Z., Ikawati, M., Tocharus, J., Kawaichi, M., Oka, C., 2015. Abnormal development of placenta in HtrA1-deficient mice. Dev. Biol. 397 (1), 89–102.

Hayward, C.E., Lean, S., Sibley, C.P., Jones, R.L., Wareing, M., Greenwood, S.L., Dilworth, M.R., 2016. Placental Adaptation: What Can We Learn from Birthweight: Placental Weight Ratio? Front. Physiol. 7, 28.

Hernandez, R., Li, X., Shi, J., Dave, T.R., Zhou, T., Chen, Q., Zhou, C., 2024. Paternal hypercholesterolemia elicits sex-specific exacerbation of atherosclerosis in offspring. JCI Insight 9 (17).

Hong, Z., Xu, Y., Wu, J., 2024. Bisphenol A: Epigenetic effects on the male reproductive system and male offspring. Reprod. Toxicol. 129, 108656.

Houston, B.J., Nixon, B., King, B.V., De Iuliis, G.N., Aitken, R.J., 2016. The effects of radiofrequency electromagnetic radiation on sperm function. Reproduction 152 (6), R263–R276.
International Commission on Non-Ionizing Radiation, P., 2020. Guidelines for Limiting Exposure to Electromagnetic Fields (100 kHz to 300 GHz). Health Phys. 118 (5), 483–524.
Jaffar, F.H.F., Osman, K., Ismail, N.H., Chin, K.Y., Ibrahim, S.F., 2019. Adverse Effects of Wi-Fi Radiation on Male Reproductive System: A Systematic Review. Tohoku J. Exp. Med. 248 (3), 169–179.
Jodar, M., 2019. Sperm and seminal plasma RNAs: what roles do they play beyond fertilization? Reproduction 158 (4), R113–R123.
Kesari, K.K., Behari, J., 2012. Evidence for mobile phone radiation exposure effects on reproductive pattern of male rats: role of ROS. Electromagn. Biol. Med. 31 (3), 213–222.
Khoshbakht, S., Motejaded, F., Karimi, S., Jalilvand, N., Ebrahimzadeh-Bideskan, A., 2021. Protective effects of selenium on electromagnetic field-induced apoptosis, aromatase P450 activity, and leptin receptor expression in rat testis. Iran. J. Basic. Med. Sci. 24 (3), 322–330.
Kitamura, A., Miyauchi, N., Hamada, H., Hiura, H., Chiba, H., Okae, H., Sato, A., John, R. M., Arima, T., 2015. Epigenetic alterations in sperm associated with male infertility. Congenit. Anom. (Kyoto) 55 (3), 133–144.
Liao, H., Lu, D., Reisinger, S.N., Mehrabadi, M.R., Gubert, C., Hannan, A.J., 2025. Epigenetic effects of paternal environmental exposures and experiences on offspring phenotypes. Trends Genet. 41 (9), 735–761.
Macrae, T.A., Fothergill-Robinson, J., Ramalho-Santos, M., 2023. Regulation, functions and transmission of bivalent chromatin during mammalian development. Nat. Rev. Mol. Cell. Biol. 24 (1), 6–26.
Maluin, S.M., Jaffar, F.H.F., Osman, K., Zulkefli, A.F., Mat Ros, M.F., Ibrahim, S.F., 2024. Exploring edible bird nest's potential in mitigating Wi-Fi's impact on male reproductive health. Reprod. Med. Biol. 23 (1), e12606.
Mehta, J., Khira, R., Fumakiya, S., Sharma, P., Punekar, A., Jain, C., Uggini, G.K., 2025. From adults to offspring: Wi-Fi RF-EMR exposure in adult zebrafish impairs reproduction and transgenerationally effects development and behavior of progeny. Sci. Total. Environ. 1008, 180982.
Melnick, R.L., Moskowitz, J.M., Heroux, P., Mallery-Blythe, E., McCredden, J.E., Herbert, M., Hardell, L., Philips, A., Belpoggi, F., Frank, J.W., Scarato, T., Kelley, E., 2025. F. International Commission on the Biological Effects of Electromagnetic, The WHO-commissioned systematic reviews on health effects of radiofrequency radiation provide no assurance of safety. Environ. Health 24 (1), 70.
Millan-Zambrano, G., Burton, A., Bannister, A.J., Schneider, R., 2022. Histone post-translational modifications - cause and consequence of genome function. Nat. Rev. Genet. 23 (9), 563–580.
Mjoen, G., Saetre, D.O., Lie, R.T., Tynes, T., Blaasaas, K.G., Hannevik, M., Irgens, L.M., 2006. Paternal occupational exposure to radiofrequency electromagnetic fields and risk of adverse pregnancy outcome. Eur. J. Epidemiol. 21 (7), 529–535.
Moazamian, A., Saez, F., Drevet, J.R., Aitken, R.J., Gharagozloo, P., 2025. Redox-Driven Epigenetic Modifications in Sperm: Unraveling Paternal Influences on Embryo Development and Transgenerational Health. Antioxidants 14 (5).
Mokarram, P., Sheikhi, M., Mortazavi, S.M.J., Saeb, S., Shokrpour, N., 2017. Effect of Exposure to 900 MHz GSM Mobile Phone Radiofrequency Radiation on Estrogen Receptor Methylation Status in Colon Cells of Male Sprague Dawley Rats. J. Biomed. Phys. Eng. 7 (1), 79–86.
Pall, M.L., 2018. Wi-Fi is an important threat to human health. Environ. Res. 164, 405–416.
Park, S.H., Pan, J., Zhang, X., Lin, T.A., Tang, S., Li, X., Cheloufi, S., Chen, Q., Zhou, T., Zhou, C., 2026. Paternal Microplastic Exposure Alters Sperm Small Noncoding RNAs and Affects Offspring Metabolic Health in Mice. J. Endocr. Soc. 10 (2), bvaf214.
Rampon, C., Bouillot, S., Climescu-Haulica, A., Prandini, M.H., Cand, F., Vandenbrouck, Y., Huber, P., 2008. Protocadherin 12 deficiency alters morphogenesis and transcriptional profile of the placenta. Physiol. Genom. 34 (2), 193–204.
Ren, L., Xin, Y., Sun, X., Zhang, Y., Chen, Y., Liu, S., He, B., 2022. Small Noncoding RNAs Contribute to Sperm Oxidative Stress-Induced Programming of Behavioral and Metabolic Phenotypes in Offspring. Oxid. Med. Cell. Longev. 2022, 6877283.
Sabari, B.R., Zhang, D., Allis, C.D., Zhao, Y., 2017. Metabolic regulation of gene expression through histone acylations. Nat. Rev. Mol. Cell. Biol. 18 (2), 90–101.
Sage, C., Burgio, E., 2018. Electromagnetic Fields, Pulsed Radiofrequency Radiation, and Epigenetics: How Wireless Technologies May Affect Childhood Development. Child. Dev. 89 (1), 129–136.
Sakhaee, E., Emadi, L., Azari, O., Kheirandish, R., Esmaili Nejad, M.R., Shafiei Bafti, H., 2016. Effects of Cuminum cyminum L. essential oil on some epididymal sperm parameters and histopathology of testes following experimentally induced copper poisoning in mice. Andrologia 48 (5), 542–547.
Shokri, M., Shamsaei, M.E., Malekshah, A.K., Amiri, F.T., 2020. The protective effect of melatonin on radiofrequency electromagnetic fields of mobile phone-induced testicular damage in an experimental mouse model. Andrologia 52 (11), e13834.
Skvortsova, K., Iovino, N., Bogdanovic, O., 2018. Functions and mechanisms of epigenetic inheritance in animals. Nat. Rev. Mol. Cell. Biol. 19 (12), 774–790.
Sun, C., Groom, K.M., Oyston, C., Chamley, L.W., Clark, A.R., James, J.L., 2020. The placenta in fetal growth restriction: What is going wrong? Placenta 96, 10–18.
Tomar, A., Gomez-Velazquez, M., Gerlini, R., Comas-Armangue, G., Makharadze, L., Kolbe, T., Boersma, A., Dahlhoff, M., Burgstaller, J.P., Lassi, M., Darr, J., Toppari, J., Virtanen, H., Kuhnapfel, A., Scholz, M., Landgraf, K., Kiess, W., Vogel, M., Gailus-Durner, V., Fuchs, H., Marschall, S., Hrabe de Angelis, M., Kotaja, N., Korner, A., Teperino, R., 2024. Epigenetic inheritance of diet-induced and sperm-borne mitochondrial RNAs. Nature 630 (8017), 720–727.
Trigg, N.A., Conine, C.C., 2024. Epididymal acquired sperm microRNAs modify post-fertilization embryonic gene expression. Cell. Rep. 43 (9), 114698.
Vijay, S., Ibrahim, S.F., Osman, K., Zulkefli, A.F., Mat Ros, M.F., Jamaludin, N., Syed Taha, S.M.A., Hairulazam, A., Jaffar, F.H.F., 2025. Histomorphometry and sperm quality in male rats exposed to 2.45 GHz Wi-Fi. Reproduction 169 (5).
Warkiani, M.E., Goss, D.M., 2026. An expanded paternal legacy: epididymal mRNAs are transmitted to the embryo. Nat. Rev. Urol.
Wu, Y., Wei, Y., Li, Y., Dou, Y., Yang, Y., Liu, H., Wang, X., Wang, Z., Su, J., Zhang, Y., Wang, Y., 2025. Sperm-Derived CircRNA-1572 Regulates Embryogenesis and Zygotic Genome Activation by Targeting CCNB2 via Bta-miR-2478-L-2. Adv. Sci. (Weinh.) 12 (18), e2414325.
Xavier, M.J., Roman, S.D., Aitken, R.J., Nixon, B., 2019. Transgenerational inheritance: how impacts to the epigenetic and genetic information of parents affect offspring health. Hum. Reprod. Update 25 (5), 518–540.
Yan, S., Ju, Y., Dong, J., Lei, H., Wang, J., Xu, Q., Ma, Y., Wang, J., Wang, X., 2022. Paternal radiofrequency electromagnetic radiation exposure causes sex-specific differences in body weight trajectory and glucose metabolism in offspring mice. Front. Public. Health 10, 872198.
Zhang, Y., Song, J.Y., Sun, Z.G., 2025. Exploring the impact of environmental factors on male reproductive health through epigenetics. Reprod. Toxicol. 132, 108832.